Geometry optimization to increase the flux control range of a double excitation synchronous motor

Trung-Kien Hoang, L Vido, F Gillon, M. Gabsi

GEOMETRY OPTIMIZATION TO INCREASE THE FLUX CONTROL RANGE OF A DOUBLE EXCITATION SYNCHRONOUS MOTOR

K. Hoang[1], L. Vido[2], F. Gillon[3], and M. Gabsi[1]

[1] SATIE, ENS Cachan, 94235 Cachan, France
e-mail : kienht26@gmail.com
[2] SATIE, University of Cergy-Pontoise, 33 bd du Port, 95000 Cergy-Pontoise, France
[3] L2EP, Ecole Centrale de Lille, 59650 Villeneuve d'Ascq Cedex, France

Abstract - This paper deals with a structural optimization to improve the open circuit flux control capability of a double excitation synchronous motor. In this kind of motor, the air-gap flux varies according to the field current. It can be weakened or enhanced when decreasing or increasing the field current. For a specific machine geometry, minimum and maximum air-gap flux are found at certain field currents. It is, therefore, desirable to minimize the minimum flux and maximize the maximum one to improve the controlling effectiveness of the field windings. That objective is the focus of this paper through a structural optimization. The machine is modeled by using an equivalent magnetic circuit network. Some interesting points on the non-dominated pareto front will be verified against ones obtained with the 3-D finite element method.

Keyword - Double excitation, geometry optimization, permanent magnet, synchronous motor.

1 INTRODUCTION

A Double Excitation Synchronous Motor (DESM) proposes additional excitation windings in a permanent magnet synchronous motor (PMSM) [1]. Such kind of structure combines advantages of a PMSM with the high power density and high efficiency, and an advantage from a would field synchronous motor, which is capable of regulating flux in the air-gap. Several papers have been presented focusing on DESMs, such as [1–6].

In the open circuit condition, the air-gap flux varies as a function of the field current with minimum and maximum values exist in the flux weakening and flux enhancing regions, respectively. Various researches have been done in order to optimize the air-gap flux characteristic. In this paper, optimizing the air-gap flux characteristic is meant to minimize the minimum point and maximize the maximum one. In a research conducted in [6], flux regulations of different DESM structures were compared, and the authors proposed one design, in which the air-gap excitation flux can be completely canceled. Authors of [7] showed advantages of a parallel DESM over a series one in terms of the open circuit flux control capability. In [8], the flux control range was to be maximized using a parametric design method, and thermal aspect was not considered. In this paper, an optimization applied with a parallel DESM is performed to lower the minimum flux and increase maximum one, therefore broadening the flux regulation range. Due to a huge number of model evaluations, an electromagnetic model constructed by using an equivalent magnetic circuit (EMC) method will be adopted instead of finite element method (FEM). The FEM is traditionally much preferred due to its high accuracy but the long computation time disadvantage (particularly 3-D FEM) prohibits it from using when a thousands of runs are required. This paper will be constructed as follows: firstly, a reference DESM and the flux control range of the prototype are presented. Secondly, the optimization problem formulation is discussed. Then, optimization results using the multi-objective particles swarm optimization (MOPSO) approach is discussed, and some interesting points on the pareto front result are studied and compared with ones obtained by a 3-D FEM.

2 DESM PROTOTYPE

2.1 REFERENCE PARALLEL DESM MODEL

A number of motor prototypes using the double principle has been realized according to different criteria. Concerning the localization of the excitation flux sources, both sources can be placed on the stator and/or rotor. Regarding how flux sources are combine, a DESM could be classified as series or parallel ones. Fig. 1 shows the DESM reference model to be analyzed in this paper [2].

This reference topology belongs to the parallel type, which was proved to be advantegous over the series configuration in respect of controlling the open circuit

flux [7]. The main reason for choosing the parallel type is due to the fact that the main flux path generated by the field winding does not pass through permanent magnets (PMs). Although owing to a complex flux paths as presented in [2], the homopolar flux still passes the PMs causing a risk of demagnetization, and it also reduces the controlling effectiveness of the field windings. In this prototype, two toroidal field windings are placed on the stator, so it helps to avoid sliding contacts. Ferrite PMs are located in the rotor using the flux concentration principle to increase the air-gap flux. In this prototype, some flux lines are truly three dimensional as detailed in [2], so that solid core material are advised to employ in some regions. Detailed parameters are given in Table. 1

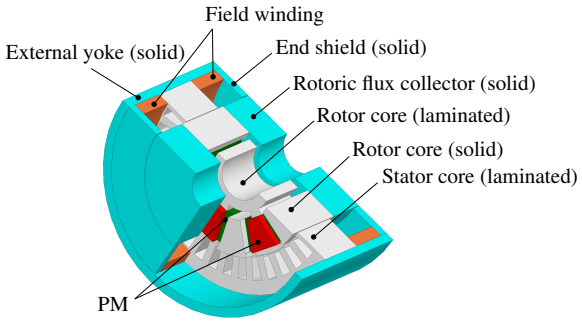

Fig. 1. Reference model of DESM.

I. Reference DESM model configuration

Parameters	Value
Number of phases	3
Number of turns per phase	33
Number of turns per field winding	150
Number of poles	12
Motor length	115 mm
Outer stator diameter	92 mm
Inner stator diameter	57.5 mm
Number of slots	36
Air-gap length	0.5 mm
PM residual flux density	0.4 T (ferrite PM)
Based speed	2000 rpm
Rated power	3 kW

2.2 Flux control range of the prototype

As mentioned, the purpose of this paper is to optimize the open circuit air-gap flux characteristic. Therefore, an examination of this curve with the reference model is shown in Fig. 2. This is obtained by using the EMC method [9]. On account of the thermal limit, the field current will vary between -6 A (weakening) and 6 A (enhancing). The EMC results agree well with ones obtained by using Ansys Maxwell, which is a 3-D FEM package. It is interesting to see an unwanted reducing effect on the flux when the field current reaches high. This is explained by the homopolar configuration, which causes differencet effects of field current on two stator tooth groups: the first group increases flux and the second one decreases flux when field current increases. With small field current, the increasing effect of first group is bigger than reducing effect of the second one making the total flux linkage increases. However, because of the saturation when the field current significantly increases, a small increase effect is reported for the first group while the second group still decrease flux at the same rate, therefore the resultant effect make the total flux decreases. Details about flux paths are referred to [2]. Table. 2 summaries the comparison between results obtained by the EMC and 3-D FEM.

II. Flux control summary

Unit: mWb	EMC	3-D FEM
Minimum flux $\psi_{\min}$	1.13	0.95
Maximum flux $\psi_{\max}$	4.24	4.16
Range $\Delta\psi$	3.11	3.21

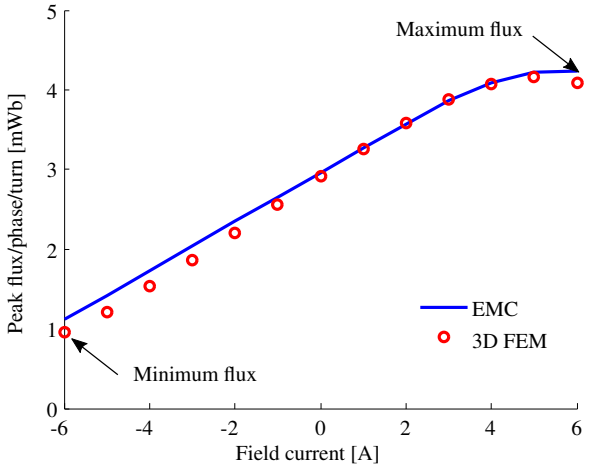

Fig. 2. Flux characteristic according to the field current.

In next section, the optimization to maximize the maximum flux and minimize the minimum flux using this EMC model will be discussed.

3 Optimization Problem Formulation

3.1 Field current range for objective calculation

With regards to the field current variation, the minimum and maximum points varies according to different machine geometries. With the reference geometry for instance, as observed in Fig. 2, the minimum and maximum points occur at field currents of approximately -6 A and 5 A, respectively. A highly accurate method

to find these minimum and maximum points is to run an optimization. However, this strategy is time consuming. Instead, a set of discrete field currents will be examined. This approach promises a good accuracy due to a simple variation of flux with respect to field current. In detail, data is sampled with the current interval of 1 A. For the range $[-6\ A \div 6\ A]$, 13 runs are required.

3.2 Problem Formulation

The optimization is formulated as (1) with the note that the maximizing ψ_{max} objective is transformed to minimizing $-\psi_{\text{max}}$ to have a min-min optimization problem which is common in optimization demonstrations.

$$\begin{aligned}
&\underset{X}{\text{Minimize}}\ F(X) = \begin{bmatrix} f_1(X) \\ f_2(X) \end{bmatrix} = \begin{bmatrix} \psi_{\text{min}} \\ -\psi_{\text{max}} \end{bmatrix} \\
&\text{s.t. } R_{\text{out}} = 92.5 \text{ mm} \\
&\quad AL = 115 \text{ mm} \\
&\quad \text{Torque} \geq 10 \text{ Nm with } J_{\text{max}} = 10 \text{ A/mm}^2 \\
&\text{with } X = [x_1, x_2, x_3, x_4, x_5, x_6] \\
&\quad 20 \text{ mm} \leq x_1 \leq 40 \text{ mm} \quad 3 \text{ mm} \leq x_4 \leq 10 \text{ mm} \\
&\quad 3 \text{ mm} \leq x_2 \leq 10 \text{ mm} \quad 3 \text{ mm} \leq x_5 \leq 7 \text{ mm} \\
&\quad 4 \text{ mm} \leq x_3 \leq 10 \text{ mm} \quad 10 \text{ mm} \leq x_6 \leq 20 \text{ mm}
\end{aligned} \tag{1}$$

where J_{max} is maximum current density (applied for both field and phase windings).
x_1, x_2, x_3, x_4, x_5, x_6 are bridge length (distance between laminated stator and end-shield), bridge thickness (same as the end-shield thickness), azimuth PM thickness, side PM thickness, stator tooth width and stator tooth length, respectively in Fig. 1.
R_{out} and AL are outer radius and axial length of the motor. It is important to underline that R_{out} and AL are remained constant, hence, the motor volume is essentially constant. The axial length involves the axial length of laminated stator part-namely stack length (SL), bridge length (x_1) and bridge thickness (x_2). SL could be deduced from AL by (2):

$$AL = SL + 2(x_1 + x_2) \tag{2}$$

The torque constraint is examined at the maximum allowable field and phase currents (at $J_{\text{max}} = 10$ A/mm^2).

4 Optimization Result and 3-D FEM Validation

4.1 Optimization Result

In this research, the multi-objective particle swarm optimization (MOPSO) is used [10,11]. This optimization technique is an evolutionary computation optimization (a search method based on a natural system) developed by Kennedy and Eberhart [12–14]. In this paper, the number of generations and swarm size are both chosen as 50. The optimization pareto front result is presented in Fig. 3. The convergence of the pareto front is also displayed for the first, 15th, 30th, and 50th (the last) generations. The range of flux control, i.e. the difference between maximum flux and minimum flux, is shown in Fig. 4.

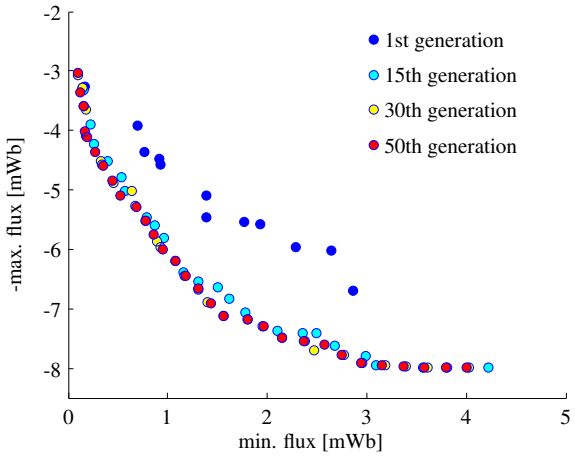

Fig. 3. Non-dominated solution at different generations

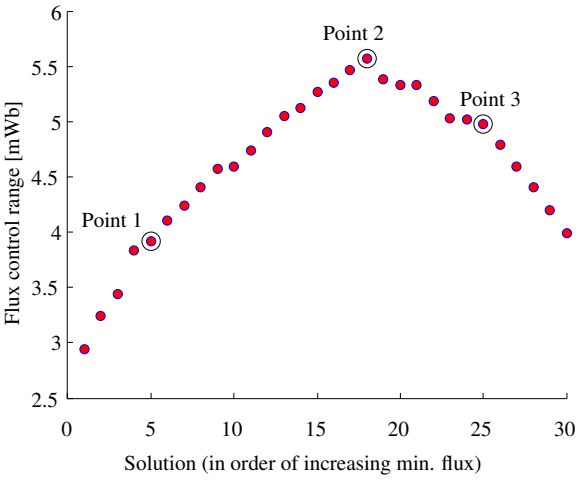

Fig. 4. Range of flux control at final generation on the pareto front

There are three interesting points on the pareto front, the first point (the left extreme in Fig. 3) corresponds to a structure, where the minimum flux is close to zero i.e. the field windings almost cancel out the flux from PMs. The second one is where the range of flux control gets maximum and the last one (on the extreme right in Fig. 3) is where the maximum flux reaches maximum. However, for the first 5 points on the left, the minimizing ψ_{min} objectives are almost the same while much improvement is seen for minimizing $-\psi_{\text{max}}$ from the first to the last. Therefore, the first 4 points on the left are proposed to remove. The same approach is applied for the last 6 point group on the right: almost no improvement for minimizing $-\psi_{\text{max}}$ and minimizing ψ_{min} objective much decreases. As the result, the

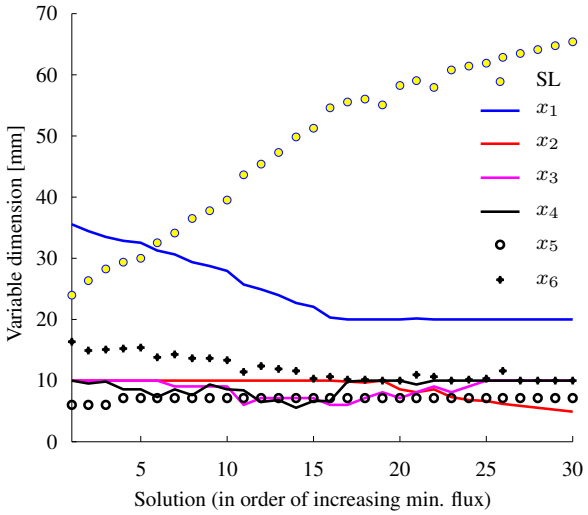

Fig. 5. Variable changes along the pareto front

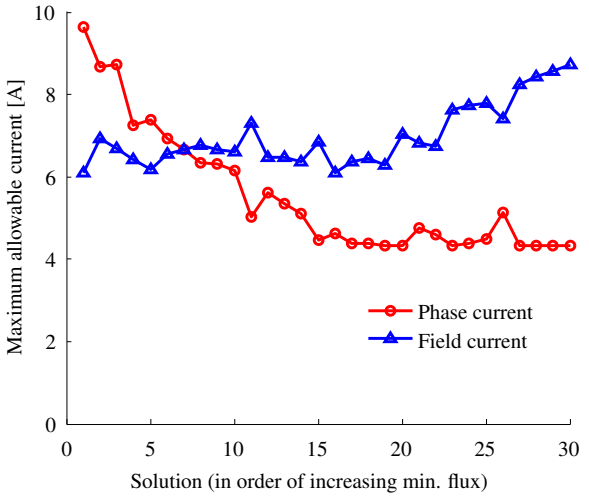

Fig. 6. Maximum allowable currents along the pareto front

last 5 points on the right are proposed to remove. In these non-dominated solutions, there does not exist any one better than other in all objectives. In other words, there is no way to compare them all. However, three interesting points are selected for further analysis and validated with 3-D FEM, in particularly: the two extreme points (on the left - Point 1 and right - Point 3) together with the point of maximum flux control range - Point 2.

The variable changes and stack length (SL) (described as (2)) according to solutions on the pareto front are sketched in Fig. 5. As reported in Fig. 5, the stack length (SL) reveals an increasing trend as both objectives increase. This could be generally explained by the fact that when the stack length increases, it causes the azimuth PM length (these PMs are attached along the stack length) increases, hence more flux from these PMs.

As described in section 3.2, the torque constraint is examined at maximum allowable field and phase currents. These maximum values at each given solution occur at maximum current density $J_{max} = 10$ A/mm^2. Their evolution is depicted in Fig. 6. As it will be seen: a decreasing trend for the phase current and a slight increasing trend for field current. Together with variables trend shown in Fig. 5, it can be observed that although the stack length expands, the available space in axial direction for the field windings is reduced due to relation (2). However, the stator tooth length (x_6) decreases i.e. more spaces for the field windings in the radial direction. The radial expansion takes dominance over the axial one, as a result, more spaces for the field windings. Meanwhile, the stator tooth width (x_5) reaches and remains at its maximum value (7 mm) leading to a reduction of the phase winding slot area when the stator tooth length is shortened.

4.2 3-D FEM VALIDATION

As mentioned above, three points of interest will be examined by comparisons with 3-D FEM for theirs flux control capabilities. Table. 3 summaries dimensions of these points in comparison with the reference model. The corresponding geometries will be seen in Fig. 7

III. Variables of interested points

Unit: mm	Point 1	Point 2	Point 3	Reference
SL	30	55.8	61.8	40
x_1	32.5	20	20	30.5
x_2	10	9.6	6.6	7
x_3	10	7	10	6
x_4	8.5	10	10	6
x_5	7	7	7	5.5
x_6	15.3	10.1	10.3	17.5

The FEM validation of flux control capabilities over the field current range of $[-6\ A \div 6\ A]$ is presented in Fig. 8 together with the reference model.

A good accordance between the EMCN models and 3-D FEM ones is seen in Fig. 8. Point 2 (maximum flux control ranges) exhibits its highest slope i.e. better efficiency of the field current utilization in the flux regulation. Table. 4 (3-D FEM result) compares the flux control characteristics of the three points and the reference model.

5 CONCLUSION

An optimization using MOPSO strategy with EMCN model has been presented in this paper. The optimization purpose focuses on improving flux control range of a type of DESM. Several solutions are proposed with

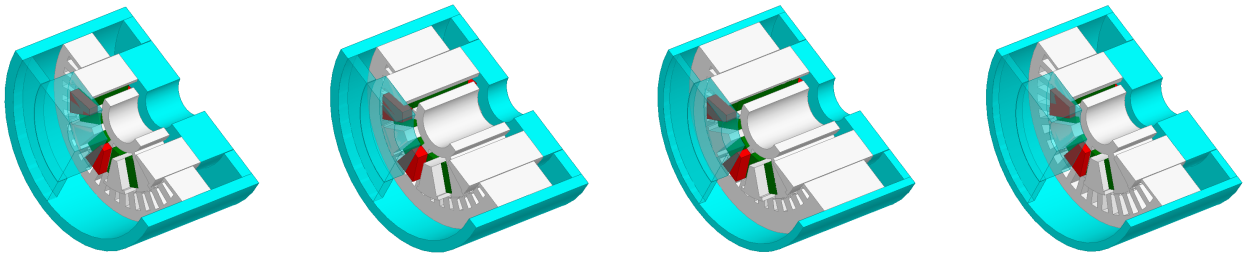

(a) (b) (c) (d)

Fig. 7. Corresponding geometries: (a) Point 1. (b) Point 2. (c) Point 3. (d) Reference model

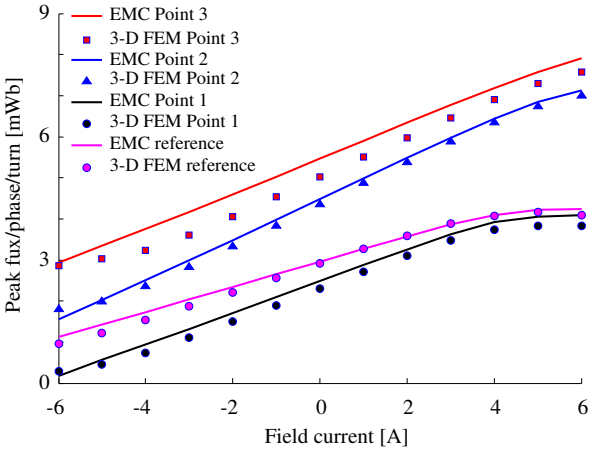

Fig. 8. Result validations with 3-D FEM ones.

IV. Flux control summary (3-D FEM result)

Unit: mWb	Point 1	Point 2	Point 3	Reference
$\psi_{\min}$	0.28	1.79	2.87	0.95
$\psi_{\max}$	3.84	7.00	7.57	4.16
$\Delta\psi$	3.56	5.21	4.70	3.21

one could improve flux control range from 3.21 mWb (reference model) to 5.21 mWb with the same range of field current. One configuration is also found to almost cancel out PM flux. These findings further emphasizes a distinguishing feature of air-gap flux adjustment by field windings in DESMs. In a perspective, performance comparisons will be considered to comprehensively evaluate the proposed models.

References

[1] Y. Amara, L. Vido, M. Gabsi, E. Hoang, A. Hamid Ben Ahmed, and M. Lecrivain, "Hybrid excitation synchronous machines: Energy-efficient solution for vehicles propulsion," *Vehicular Technology, IEEE Transactions on*, vol. 58, no. 5, pp. 2137–2149, Jun 2009.

[2] L. Vido, M. Gabsi, M. Lecrivain, Y. Amara, and F. Chabot, "Homopolar and bipolar hybrid excitation synchronous machines," in *Electric Machines and Drives, 2005 IEEE International Conference on*, May 2005, pp. 1212–1218.

[3] E. Hoang, M. Lecrivain, and M. Gabsi, "A new structure of a switching flux synchronous polyphased machine with hybrid excitation," in *European Conference on Power Electronics and Applications*, Sept. 2007, pp. pp.1–8.

[4] D. Fodorean, A. Djerdir, I. A. Viorel, and A. Miraoui, "A double excited synchronous machine for direct drive application: Design and prototype tests," *Energy Conversion, IEEE Transactions on*, vol. 22, no. 3, pp. 656–665, Sept 2007.

[5] R. Owen, Z. Zhu, and G. Jewell, "Hybrid-excited flux-switching permanent-magnet machines with iron flux bridges," *Magnetics, IEEE Transactions on*, vol. 46, no. 6, pp. 1726–1729, June 2010.

[6] B. Nedjar, S. Hlioui, Y. Amara, L. Vido, M. Gabsi, and M. Lecrivain, "A new parallel double excitation synchronous machine," *Magnetics, IEEE Transactions on*, vol. 47, no. 9, pp. 2252–2260, Sept 2011.

[7] Y. Amara, S. Hlioui, R. Belfkira, G. Barakat, and M. Gabsi, "Comparison of open circuit flux control capability of a series double excitation machine and a parallel double excitation machine," *Vehicular Technology, IEEE Transactions on*, vol. 60, no. 9, pp. 4194–4207, Nov 2011.

[8] K. Hoang, L. Vido, M. Gabsi, and F. Gillon, "Flux control range broadening and torque ripple minimization of a double excitation synchronous motor," *IEEE Transactions on Magnetics*, vol. 53, no. 1, pp. 1–10, Jan 2017.

[9] K. Hoang, L. Vido, F. Gillon, and M. Gabsi, "Modeling of double excitation synchronous motors using nodal based generalized equivalent magnetic circui." ISEF, September 2015.

[10] J. Aubry, H. B. Ahmed, and B. Multon, "Bi-objective sizing optimization of a pm machine

drive on an operating profile," in *Electrical Machines (ICEM), 2010 XIX International Conference on*, Sept 2010, pp. 1–7.

[11] J. Aubry, "Optimisation du dimensionnement d'une chaîne de conversion électrique directe incluant un système de lissage de production par supercondensateurs. application au houlogénérateur searev," Thèse, École normale supérieure de Cachan - ENS Cachan, Nov. 2011.

[12] J. Kennedy and R. Eberhart, "Particle swarm optimization," in *Neural Networks, 1995. Proceedings., IEEE International Conference on*, vol. 4, Nov 1995, pp. 1942–1948 vol.4.

[13] Y. Shi and R. Eberhart, "Empirical study of particle swarm optimization," in *Evolutionary Computation, 1999. CEC 99. Proceedings of the 1999 Congress on*, vol. 3, 1999, pp. –1950 Vol. 3.

[14] R. Eberhart and Y. Shi, "Particle swarm optimization: developments, applications and resources," in *Evolutionary Computation, 2001. Proceedings of the 2001 Congress on*, vol. 1, 2001, pp. 81–86 vol. 1.